The analytical solution of the grouting migration height for the post-grouted drilled shaft based on the Herschel-Bulkley model

Gan Nan[a], Hai-ming Liu[a,*], Yan-jie Zhang[b], Wen-yun Ding[c], Jing Cao[a], Rong-tao Yan[d,*]

[a] *Faculty of Civil Engineering and Mechanics, Kunming University of Science and Technology, Kunming, Yunnan 650224, PR China;*

[b] *YCIH Foundation Engineering Co., Ltd., Kunming, Yunnan 650501, PR China;*

[c] *China railway Er-yuan engineering group Co. Ltd, Kunming 650500, PR China;*

[d] *Guangxi Key Laboratory of New Energy and Building Energy Saving, Guilin University of Technology, Guilin, Guangxi 541004, PR China*

[*] *Correspondence should be addressed to Haiming Liu hmliu@kust.edu.cn and Rongtao Yan yrt301@163.com*

ABSTRACT: The traditional bored pile technology has some arduous problems, such as the sediment at the pile tip, the mud skin along the pile shaft, and the stress release due to borehole construction. The post-grouted technology at the pile tip of bored pile has emerged because of demand. The grouting migration height (GMH) is of great significance to the strengthen and reinforcement of the pile foundation. This paper derives the calculation formula of the GMH based on the theory of the column hole expansion and Herschel-Bulkley model. The influence of relevant parameters on the GMH is discussed. Aiming at the problem of the grouting migration along the pile shaft in layered soils, the iterative calculation method of the GMH is proposed. The correctness of the GMH is verified by an engineering case, which can guide the engineering practice. The result shows that the GMH increases with the increase of the grouting pressure, the pile diameter and the thickness of the mud skin, and the grouting pressure is positively correlated with the GMH. The GMH decreases with the increase of the buried depth, the consistency coefficient and the rheological index. On this basis, the correctness of the GMH is verified by an engineering case.

Keywords: Grouting migration height; Herschel-Bulkley model; Post-grouted drilled shafts; Layered soils; Iterative calculation method

1. Introduction

The bored cast-in-place concrete piles have many advantages, such as the high bearing capacity of the single pile, the flexible selection for the pile length and diameter, and the wide adaptability to various soil conditions [1]. Thus, it has been widely used in the pile foundation

 doi:10.20944/preprints202109.0011.v1

engineering of high-rise buildings, highway bridges, high-speed railways, transmission towers and so on [2, 3]. However, there are some problems encountered in the construction and the use of the bored cast-in-place concrete pile. The first problem is the reduction in the side friction of the bored cast-in-place concrete pile resulting from the existence of the mud skin and the stress relaxation of the soil at the pile shaft due to mud protection measures and the borehole disturbance [4]. Secondly, the difficulties in the hole clearing at the pile tip and construction disturbances perhaps lead to the sediment and soil softening, which causes the resistence reduction at the pile tip [5]. The end resistance of the pile is unable to be allowed full play because of the softening conditions of the pile tip, and the occuring displacement of the pile tip is 10-30 times as large as the displacement of the pile shaft studied by Safaqah et al. [6]. To effectively solve this problem, the post-grouted drilled shaft (PGDS) has become an effective method. The grouting material is injected into the soils of the pile tip and the pile shaft through the pre-embedded grouting pipe, the strength of soils at the pile tip and the pile shaft can be significantly enhanced [7].

In 1958, the PGDS was first introuduced into the construction of the pile foundation of Maracaibo Bridge in Venezuela. Subsequently, the PGDS has been gradually innovated and developed in the pile foundation engineering, mainly including the Gravel Basket Device [8], the High Pressure Bi-directional Loading Cells [9], the Sleeve Valve Tube Grouting Device [10], the Frustum Confining Vessel [11, 12], the U-shaped Tube Grouting Device [13], the Punching and Binding Grouting Technology [14], and the Reserved Cavity Grouting with Movable Steel Plate [15]. Many researchers have carried out field or model tests to measure its bearing capacity of the PSDS [16-18]. Meanwhile, the reinforcing mechanism of the PGDS has been revealed, which mainly consists of the reinforcement effect of grouting material on soil at the pile tip [19-21], the enlargement of the pile tip [22, 23], the reinforcement effect of grouting split along the pile shaft [24, 25], and the negative friction of the pile shaft caused by grouting [26, 27]. However, resulting from the complexity of influencing factors of the PGDS and the diversity of reinforcement methods, the current theoretical research of the PGDS lags far behind the engineering practice.

In the process of the PGDS, the grouting material will infiltrate into the surrounding rock and soil under the grouting pressure. With the increasing of the grouting pressure, the grouting material will compact the rock and soil. When the grouting pressure reaches the splitting strength of the rock and soil, the grouting material will penetrate along the mud skin, which plays an

 doi:10.20944/preprints202109.0011.v1

important role in the overall reinforcement for the soil of the pile shaft and pile tip of the bored cast-in-place concrete pile. Therefore, the grouting split theory is the crux of determining the grouting migration height (GMH). The research of the grouting split theory mainly includes the split mechanism and the propagation mode. The split mechanism is mainly concerned with the starting split conditions and the threshold of split pressure [28, 29]. The empirical solutions are obtained by the model test or field test [30-32], and the analytical solutions are deduced based on the tension failure, shear failure and other failure criteria to obtain theoretical models [33, 34]. For the propagation paths characteristics of the grouting split, Li et al. [35], Zou et al. [36] and Zhang et al. [37] adopt constitutive models of the Newtonian fluid, the Bingham fluid or the Power-law fluid to obtain the relationship between the diffusion radius of the grouting split and the grouting pressure respectively. Because the propagation paths of split have complex dynamic properties and the research is highly complex, tentative studies are carried out using the numerical simulation and model tests. Yang [38], Murdoch [39] and Bezuijen [40] carried out laboratory simulation experiments of the grouting split path propagation using the grouting material separation and the scanning electron microscopy. Many scholars simulate the grouting split process based on the particle flow method and the discrete element software [41-44].

At present, the GMH is mostly determined by experience and differs greatly from the actual project frequently, which hinders the development of the post-grouted technology seriously. Therefore, based on the theory of the cylindrical cavity expansion, the Herschel-Bulkley model and the basic equation of the uniform flow, an equation for calculating the GMH along the mud skin of the pile shaft is derived in this paper. The influences of grouting parameters, the grouting pressure, the pile length, the pile diameter and the mud thickness on the GMH are analyzed emphatically. Furthermore, the proposed method is validated through the comparison with the observation data in an engineering case. This study provides the theoretical foundation for further study and the application of the post-grouted technology.

2. Study on the grouting split of the Herschel-Bulkley model

2.1. The basic hypothesis of the PSDS

The basic assumptions of the grouting split in soils are as follows: (1) The grouting material conforms to the Herschel-Bulkley model and the flow pattern of the grouting material remains unchanged during grouting. (2) The grouting material is an incompressible homogeneous isotropic

Preprints (www.preprints.org) | NOT PEER-REVIEWED | Posted: 1 September 2021 doi:10.20944/preprints202109.0011.v1

fluid without considering the time-varying effect of the grouting material. (3) The fracture aperture and the velocity of the grouting material are small. The flow pattern of grouting material is the laminar flow. (4) When the grouting material flows in the aperture, the no-slip condition of the wall is established, i.e., the velocity of the grouting flow on the upper and lower surface of the aperture is 0. (5) The treated soil is considered as an isotropic homogeneous material. (6) It is assumed that the consistency coefficient of the grouting material is constant in the course of the movement. (7) The pile shaft is a regular cylindrical surface regardless of the roughness of the pile shaft. (8) The aperture width of the grouting split is $b + u_i$, where b is the thickness of the mud skin, and u_i is the compression of the soil and mud skin at the pile shaft in section i. (9) The grouting material has good grouting ability and no blockage occurs, i.e., the effect of the pressure filtration is not considered.

2.2. Theoretic derivation

(1) Theoretical deduction of the soil at the pile shaft

In the process of the grouting split, the lateral displacement of the soil at the pile shaft is produced. According to the theory of the cylindrical cavity expansion, the calculation of the lateral displacement can be simplified as the axisymmetric plane problem, whose calculation model is shown in Fig. 1-(a) and Fig. 1-(b). There is no shear stress on the θ plane, i.e. $\tau_{\theta r} = \tau_{\theta z} = 0$. Furthermore, the stress change in the z direction is not considered. According to the force balance in the direction of radius r, Equation (1) can be obtained.

$$\left(\sigma_r + \frac{\partial \sigma_r}{\partial r}\mathrm{d}r\right)(r + \mathrm{d}r)\mathrm{d}\theta\mathrm{d}z - \sigma_r r\mathrm{d}\theta\mathrm{d}z + \left(\tau_{zr} + \frac{\partial \tau_{zr}}{\partial z}dz\right)\left(r + \frac{dr}{2}\right)\mathrm{d}\theta\mathrm{d}r - \tau_{zr}\left(r + \frac{dr}{2}\right)\mathrm{d}\theta\mathrm{d}r - 2\sigma_\theta \mathrm{d}r\mathrm{d}z \cdot \sin\frac{\mathrm{d}\theta}{2} = 0, \quad (1)$$

where σ_r is the radial stress, σ_θ is the tangential stress, r is the radius of the calculation point and τ_{ij} is the shear stress, which i denotes the normal direction of the stress action plane and j denotes the direction of the stress action.

By simplifying Equation (1) and omitting higher-order infinitesimal quantities, we can obtain

$$\frac{\mathrm{d}\sigma_r}{\mathrm{d}r} + \frac{\sigma_r - \sigma_\theta}{r} = 0. \quad (2)$$

Preprints (www.preprints.org) | NOT PEER-REVIEWED | Posted: 1 September 2021 doi:10.20944/preprints202109.0011.v1

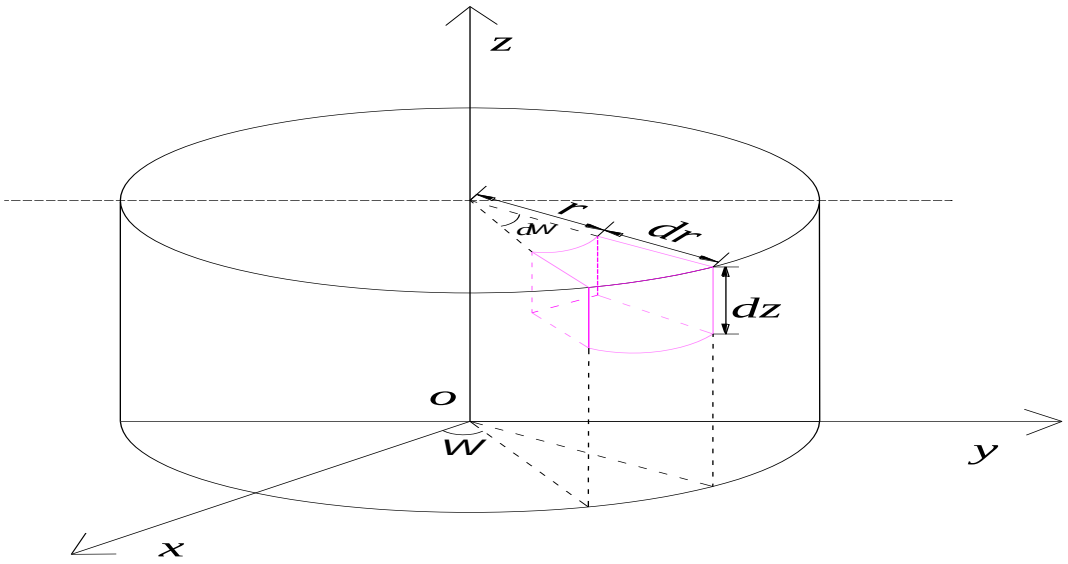

(a) The diagram for selecting the soil element at the pile shaft.

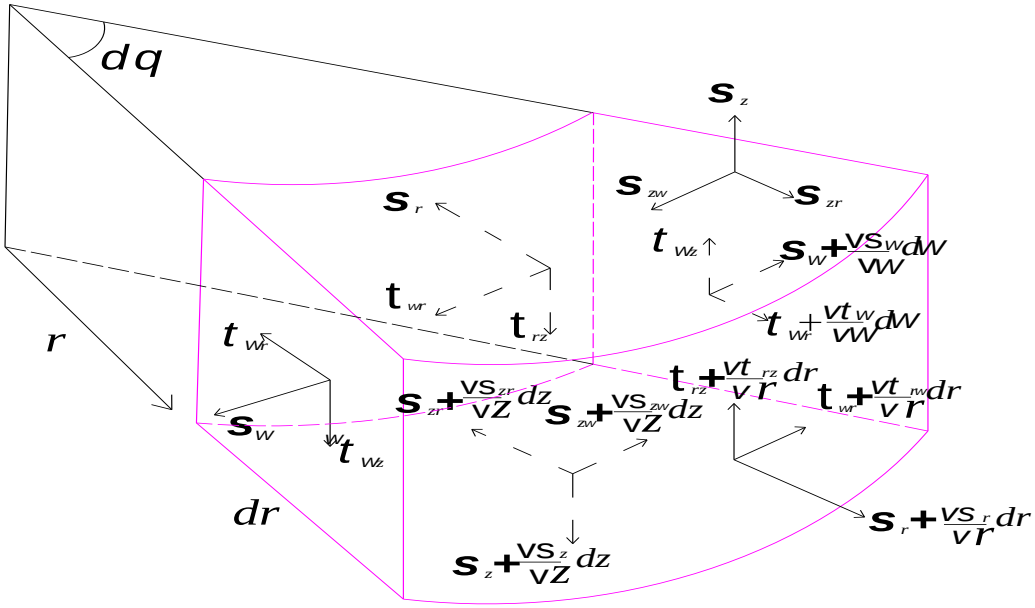

(b) The diagrammatic sketch of the force acting on the soil element.

Fig. 1. The computational model of the soil element.

According to the geometric equation, we have

$$\begin{cases} \varepsilon_r = \dfrac{\mathrm{d}u_r}{\mathrm{d}r} \\ \varepsilon_\theta = \dfrac{u_r}{r} \end{cases}, \tag{3}$$

where ε_r is the radial strain, ε_θ is the tangential strain, and u_r is the radial displacement.

According to the generalized Hooke's law, we obtain

$$\begin{cases} \varepsilon_r = \dfrac{1-\mu^2}{E}\left(\sigma_r - \dfrac{1-\mu}{\mu}\sigma_\theta\right) \\ \varepsilon_\theta = \dfrac{1-\mu^2}{E}\left(\sigma_\theta - \dfrac{1-\mu}{\mu}\sigma_r\right) \end{cases}, \tag{4}$$

where μ is the poisson ratio and E is the modulus of the elasticity.

Preprints (www.preprints.org) | NOT PEER-REVIEWED | Posted: 1 September 2021 doi:10.20944/preprints202109.0011.v1

The boundary conditions are

$$\begin{cases} \sigma_r(a) = p \\ \lim\limits_{r\to\infty} \sigma_r = p_0, \end{cases} \tag{5}$$

where a is the radius of the inner bore, p is the grouting pressure, and p_0 is the initial stress of the soil, which can be expressed as follows

$$\mathrm{p}_0 = k_0 \sum \gamma_i z_i. \tag{6}$$

Combined with Equation (2) to Equation (6), the displacement of the soil under the elastic state can be obtained.

$$u = \frac{p-p_0}{2G}\frac{a^2}{r}, \tag{7}$$

where u is the lateral displacement of the soil, and G is the shear modulus, which can be given as follows $G = E/2(1+\mu)$.

Assuming $r = a = r_0 + b$, it can be approximated to obtain $r \approx r_0$ because of $b \ll r_0$ in Equation (7). The displacement of the soil at the pile shaft can be simplified as follows

$$u = \frac{(p-p_0)r_0}{2G}, \tag{8}$$

where r_0 is the radius of the bored cast-in-place concrete pile.

(2) The deduction theory of the GMH

At present, the Bingham model and the Power-law fluid model are mostly adopted to describe the rheology of the cement slurry at home and abroad, which cannot describe the grouting material with the yield value and the pseudo-plasticity [45, 46]. The Herschel-Bulkley model is a three-parameter rheological model with static shear stress [47], whose constitutive equation is

$$\tau = \tau_0 + K\gamma^n, \tag{9}$$

where τ is the shear stress, τ_0 is the yield stress, K is the consistency coefficient, γ is the shear rate, and n is the rheological index.

The Herschel-Bulkley model can express the characteristics of the Newton model, the Bingham model and the Power-law fluid model, which are shown in Table 1.

Table 1. The reference table of the fluid model.

	The Newton model	The Bingham fluid	The pseudo-plastic power-law model	The expansive power-law fluid model
$\boldsymbol{\tau_0}$	0	≠0	0	0
$\boldsymbol{n}$	1	1	n<1	n>1
Constitutive equation	$\tau = K\gamma$	$\tau = \tau_0 + K\gamma$	$\tau = K\gamma^n$	$\tau = K\gamma^n$

Preprints (www.preprints.org) | NOT PEER-REVIEWED | Posted: 1 September 2021 doi:10.20944/preprints202109.0011.v1

For the non-time-varying grouting material, we obtain

$$\gamma = \frac{\mathrm{d}\upsilon}{\mathrm{d}y}, \tag{10}$$

where υ is the flow rate of the grouting material.

The computational model is shown in Fig. 2. When the grouting material penetrates, the driving force and the resistance force will be equal. What's more, the grouting pressure will be zero when the GMH reaches its maximum height. According to the above conditions, Equations (11) and (12) are valid, which is shown as follows

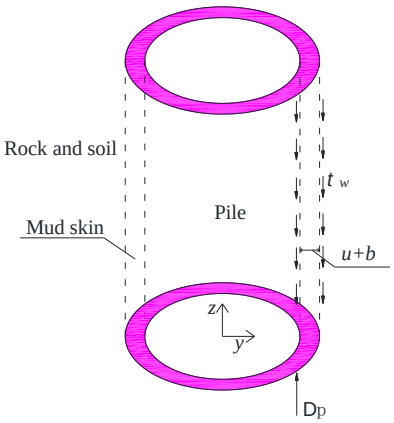

Fig. 2. The force analysis and the calculation model of grouting.

$$\Delta p \cdot y \cdot 2\pi(r_0 + y) = 2\tau \cdot 2\pi(r_0 + y) \cdot h, \tag{11}$$

and

$$\Delta p \cdot (u + b) \cdot 2\pi(r_0 + u + b) = 2\tau_e \cdot 2\pi(r_0 + u + b) \cdot h, \tag{12}$$

where Δp is the difference of the grouting pressure, and τ_e is the shear stress on the surface of the grouting material, whose flow direction is opposite to the velocity direction.

Simplifying Equations (11) and (12), we obtain

$$\tau = \frac{\Delta p y}{2h}, \tag{13}$$

and

$$\tau_e = \frac{\Delta p(u+b)}{2h}, \tag{14}$$

where h is the GMH, and τ is the shear stress at any point.

By combining Equations (9) and (10), the variables are separated by υ, and then it is integrated along the y direction. The results are as follows

$$\upsilon = -y\left(\frac{\tau-\tau_0}{K}\right)^{\frac{1}{n}} - C, \tag{15}$$

where C is a constant.

The boundary conditions are as following

Preprints (www.preprints.org) | NOT PEER-REVIEWED | Posted: 1 September 2021 doi:10.20944/preprints202109.0011.v1

$$\begin{cases} y = \frac{u+b}{2} \\ v = 0 \end{cases}. \tag{16}$$

Substituting Equation (16) into Equation (15), we have

$$C = -\frac{u+b}{2}\left(\frac{\tau-\tau_0}{K}\right)^{\frac{1}{n}}. \tag{17}$$

Substituting Equation (17) into Equation (15), we obtain

$$v = -y(\frac{\tau-\tau_0}{K})^{\frac{1}{n}} + \frac{u+b}{2}\left(\frac{\tau-\tau_0}{K}\right)^{\frac{1}{n}}. \tag{18}$$

To facilitate the derivation and the calculation of the following deduction, Equation (18) is converted into an integral form,

$$v = \int_{y}^{\frac{u+b}{2}} (\frac{\tau-\tau_0}{K})^{\frac{1}{n}} dy. \tag{19}$$

Combining with Equations (13) and (14), we have

$$y = \frac{\tau}{\tau_e}(u+b). \tag{20}$$

Substituting Equation (20) into Equation (19), the integral variable changes from y to t, and we obtain

$$v = \frac{u+b}{\tau_e}\int_{\tau}^{\frac{1}{2}\tau_e} (\frac{\tau-\tau_0}{K})^{\frac{1}{n}} d\tau. \tag{21}$$

We can derive from Equation (21),

$$v = \frac{u+b}{\tau_e}(\frac{1}{K})^{\frac{1}{n}}\frac{n}{n+1}\left[(\frac{1}{2}\tau_e - \tau_0)^{\frac{n+1}{n}} - (\tau-\tau_0)^{\frac{n+1}{n}}\right]. \tag{22}$$

Substituting Equations (13) and (14) into Equation (22), we have

$$v = \frac{u+b}{\tau_e}(\frac{1}{K})^{\frac{1}{n}}\frac{n}{n+1}\left[(\frac{\Delta p(u+b)}{4h} - \tau_0)^{\frac{n+1}{n}} - (\frac{\Delta p y}{2h} - \tau_0)^{\frac{n+1}{n}}\right]. \tag{23}$$

The flow q of the unit time is

$$q = \int_{-\frac{u+b}{2}}^{\frac{u+b}{2}} L \cdot v dy = 2L\int_{0}^{\frac{u+b}{2}} v dy. \tag{24}$$

The L in Equation (24) can be determined by

$$L = \pi r_0, \tag{25}$$

where L is the length of the aperture.

Substituting Equation (25) into Equation (24), we obtain

$$q = 2L\int_{0}^{\frac{u+b}{2}} v dy = 2\pi r_0 \int_{0}^{\frac{u+b}{2}} v dy. \tag{26}$$

Substituting Equation (23) into Equation (26), we have

$$q = 2\pi r_0 \frac{u+b}{\tau_e}(\frac{1}{k})^{\frac{1}{n}}\frac{n}{n+1}\left[\frac{u+b}{2}(\frac{\Delta p(u+b)}{4h} - \tau_0)^{\frac{n+1}{n}} - \frac{2hn}{(2n+1)\Delta p}\left(\frac{\Delta p(u+b)}{4h} - \tau_0\right)^{\frac{2n+1}{n}} + \frac{2hn}{(2n+1)\Delta p}(-\tau_0)^{\frac{2n+1}{n}}\right].$$

Preprints (www.preprints.org) | NOT PEER-REVIEWED | Posted: 1 September 2021 doi:10.20944/preprints202109.0011.v1

(27)

Substituting Equation (8) into Equation (27), we obtain

$$q=\frac{4\pi r_0 n}{n+1}\frac{h}{\Delta p}\left(\frac{1}{K}\right)^{\frac{1}{n}}\left[\frac{(p-p_0)r_0+2bG}{4G}\left(\frac{\Delta p\left((p-p_0)r_0+2bG\right)}{8Gh}-\tau_0\right)^{\frac{n+1}{n}}-\right. \quad (28)$$
$$\left.\frac{n}{2n+1}\frac{h}{\Delta p}\left(\frac{\Delta p\left((p-p_0)r_0+2bG\right)}{8Gh}-\tau_0\right)^{\frac{2n+1}{n}}+\frac{n}{2n+1}\frac{h}{\Delta p}(-\tau_0)^{\frac{2n+1}{n}}\right]$$

If the influence of the grouting material gravity is considered, Equation (29) can be obtained

$$q=\frac{4\pi r_0 n}{n+1}\frac{h}{(\Delta p-\gamma' h)}\left(\frac{1}{K}\right)^{\frac{1}{n}}\left[\frac{(p-p_0)r_0+2bG}{4G}\left(\frac{(\Delta p-\gamma' h)\left((p-p_0)r_0+2bG\right)}{8Gh}-\tau_0\right)^{\frac{n+1}{n}}-\right. \quad (29)$$
$$\left.\frac{n}{2n+1}\frac{h}{(\Delta p-\gamma' h)}\left(\frac{(\Delta p-\gamma' h)\left((p-p_0)r_0+2bG\right)}{8Gh}-\tau_0\right)^{\frac{2n+1}{n}}+\frac{n}{2n+1}\frac{h}{(\Delta p-\gamma' h)}(-\tau_0)^{\frac{2n+1}{n}}\right]$$

The difference of the grouting pressure Δp can be calculated by Equation (29).

(3) The Determination and Solution of the GMH

According to the grouting split theory, only if the grouting pressure is greater than the threshold of the split pressure, the rock and soil can be split and grouted. When the grouting pressure located at h is greater than the horizontal static earth pressure p_0, the grouting material can overcome the resistance force to split the rock and soil continuously due to the fact that the cohesion of the mud skin on the pile shaft is very small. Therefore, the GMH increases continuously. When the grouting pressure is equal to the horizontal static earth pressure, the grouting material cannot overcome the resistance force of the rock and soil. At the moment, the GMH reaches to its maximum.

$$\begin{cases} q=\dfrac{4\pi r_0 n}{n+1}\dfrac{h}{(\Delta p-\gamma' h)}\left(\dfrac{1}{K}\right)^{\frac{1}{n}}\left[\dfrac{(p-p_0)r_0+2bG}{4G}\left(\dfrac{(\Delta p-\gamma' h)\left((p-p_0)r_0+2bG\right)}{8Gh}-\tau_0\right)^{\frac{n+1}{n}}-\right. \\ \left.\dfrac{n}{2n+1}\dfrac{h}{(\Delta p-\gamma' h)}\left(\dfrac{(\Delta p-\gamma' h)\left((p-p_0)r_0+2bG\right)}{8Gh}-\tau_0\right)^{\frac{2n+1}{n}}+\dfrac{n}{2n+1}\dfrac{h}{(\Delta p-\gamma' h)}(-\tau_0)^{\frac{2n+1}{n}}\right] \\ p(0)=p \\ p(h)=p_l(h) \end{cases} \quad (30)$$

The GMH can be obtained by iterative calculation of Equation (30).

3. The iterative calculation of the GMH in layered soils

In Section 2, the formula is derived on the basis that the soil at the pile shaft is homogeneous.

Preprints (www.preprints.org) | NOT PEER-REVIEWED | Posted: 1 September 2021 doi:10.20944/preprints202109.0011.v1

In practical engineering, however, the rock and soil of the PSDS are often complex and can be simplified to multi-layered soil. The difference of mechanical properties of soils will result in the difference of the thickness of the mud skin, which will eventually affect the GMH.

The theoretical model is established to study this effect, as shown in Fig. 3. The soil along the pile shaft can be divided into n layers, and the grouting material along the pile shaft is divided into n layers according to the soil layer. The force analysis of each calculation element is also carried out. It is assumed that the grouting pressure is equal to the junctions of different calculation elements. The bottom of layer i is equal to the top of layer $i+1$, i.e., $p_i^b = p_{i+1}^t$, where p_i^b is the bottom of layer i and p_{i+1}^t is the top of layer $i+1$. The grouting pressure at the bottom of the n layer soil is equal to that at the end of the pile, i.e., $p_n^b = p$.

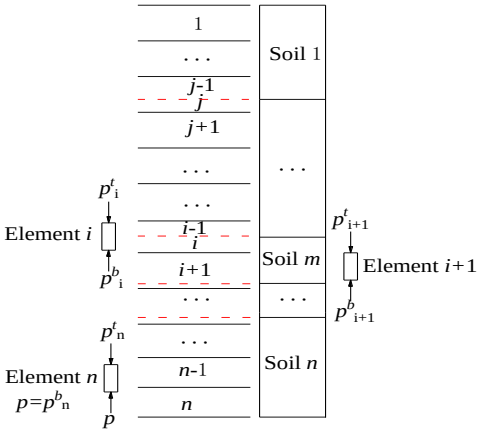

Fig. 3. The calculation model of the GMH in multi-layered soil.

According to the grouting split theory, when the grouting pressure equals the horizontal static earth pressure, the threshold of the split pressure is

$$p_s = K_0 \gamma_a (H - h), \tag{31}$$

where K_0 is the coefficient of the static earth pressure, p_s is the threshold of the split pressure at the interface of the pile-soil, and γ_a is the weighted effective weight of the soil layer above the GMH, namely, $\gamma_a = \sum_{i=1}^{h_i} \gamma_i h_i / h_i$.

According to Equation (29), the grouting pressure p_i^t at the top of section i can be calculated by Equation (32).

Preprints (www.preprints.org) | NOT PEER-REVIEWED | Posted: 1 September 2021 doi:10.20944/preprints202109.0011.v1

$$q=\frac{4\pi r_0 n}{n+1}\frac{h_i}{(p_i^b-p_i^t-\gamma' h_i)}\left(\frac{1}{K}\right)^{\frac{1}{n}}\left[\frac{(p-p_0)r_0+2bG}{4G}\left(\frac{(p_i^b-p_i^t-\gamma' h_i)\left((p-p_0)r_0+2bG\right)}{8Gh_i}-\tau_0\right)^{\frac{n+1}{n}}-\right.$$
$$\left.\frac{n}{2n+1}\frac{h_i}{(p_i^b-p_i^t-\gamma' h_i)}\left(\frac{(p_i^b-p_i^t-\gamma' h_i)\left((p-p_0)r_0+2bG\right)}{8Gh_i}-\tau_0\right)^{\frac{2n+1}{n}}+\frac{n}{2n+1}\frac{h_i}{(p_i^b-p_i^t-\gamma' h_i)}(-\tau_0)^{\frac{2n+1}{n}}\right] \quad (32)$$

In layered soils, the calculation method for the GMH is as follows, which is shown in Fig. 4.

(1) The soil along the pile shaft is divided into n layers, and the mud skin is divided into n layers according to corresponding soil layers, as shown in Fig. 3. The thickness of soil layers satisfies following conditions, $[h_i] \le H/n$. The interface of soil layers and the groundwater surface should be regarded as a stratified surface, which is shown in Fig. 3. The thickness of the calculation element in each soil layer is less than or equal to h_i.

(2) According to the condition of the grouting continuity, the grouting pressure at the bottom of section n is $p_n^b = p$. Assuming that the initial grouting hydraulic pressure on the top surface of the lowest n subsection is $p_n^{t_0}$, the $p_n^{t_1}$ can be calculated by Equation (32).

(3) Comparing $p_n^{t_0}$ with $p_n^{t_1}$, the value of $p_n^{t_1}$ is assigned to $p_n^{t_0}$ when $\left|p_n^{t_0}-p_n^{t_1}\right|>\varepsilon$. The new $p_n^{t_i}$ is calculated by Step (2) in a continuous cycle, until the two adjacent grouting pressures satisfy $\left|p_n^{t_i}-p_n^{t_{i+1}}\right| \le \varepsilon$. The final grouting pressure p_n^t on the top of the n calculation element is obtained.

(4) According to the condition of the grouting continuity, the grouting pressure at the bottom of calculation element $n-1$ is $p_{n-1}^b = p_n^t$.

(5) When the grouting pressure p_i^t at the top of calculation element i is greater than the threshold of split pressure p_s^i at the pile-soil interface of calculation element i, the next calculation element continues to calculate. If the grouting pressure p_{i+1}^t at the top of calculation element $i+1$ is greater than or equal to the grouting pressure p_i^b at the bottom of calculation element i, i.e., $p_i^t \le p_s^i$, the calculation terminates. The p_s^i is assigned to p_i^t, and the GMH of calculation element i, denoted as h_i^c, can be calculated by Equation (32).

(6) Each layer is calculated from the bottom to up according to Step (2) and (5). According to the above calculation results, the GMH is obtained as follows, $h = h_n + h_{n-1} + \cdots + h_i^c = h_i^c + \sum_{j=i+1}^{j=n} h_j$.

Preprints (www.preprints.org) | NOT PEER-REVIEWED | Posted: 1 September 2021 doi:10.20944/preprints202109.0011.v1

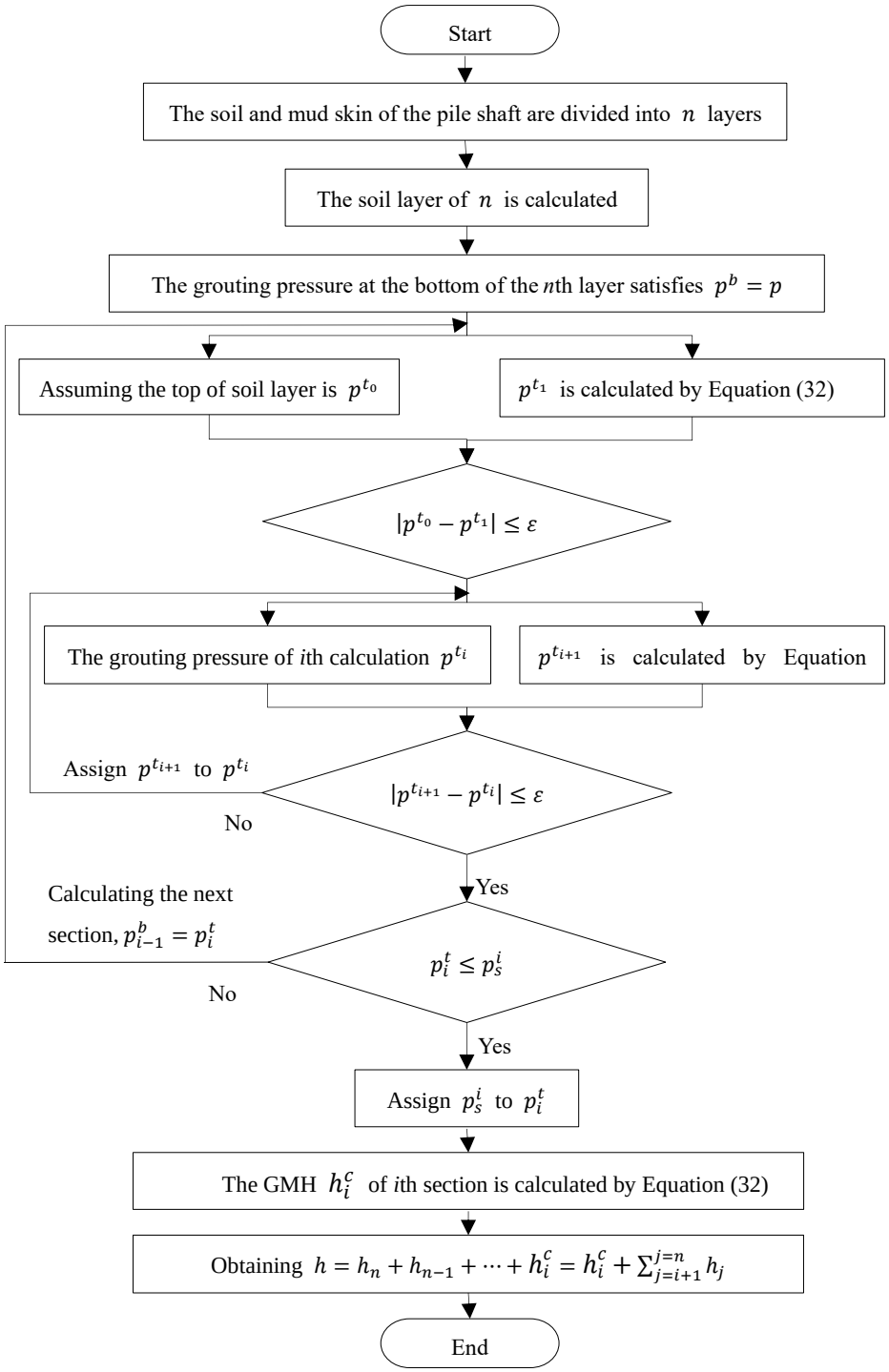

Fig. 4. The flow chart for calculating the GMH.

4. Parameter analysis

To study the influences of different parameters on the GMH, Equation (30) is solved by using the MAPLE software. It is assumed that the injected rock and soil are the homogeneous soil layer, the Poisson's ratio μ is 0.35, the weight of the soil is $\gamma = 20\text{kN/m}^3$, and the weight of the grouting material is $\gamma' = 17\text{kN/m}^3$. The static earth pressure coefficient K_0 and the deformation

Preprints (www.preprints.org) | NOT PEER-REVIEWED | Posted: 1 September 2021 doi:10.20944/preprints202109.0011.v1

modulus E of soils are shown in Table 2.

Table 2. The parameters of soils for the PGDS.

Category of the rock and soil	Gravel or pebble	Sand	Silty soil	Clay
K_0	0.20	0.25	0.40	0.55
E(MPa)	360	130	85	60

Note: The deformation modulus is larger, because the grouting time is short.

4.1. The relationship between the rheological index and the GMH

The grouting parameters are supposed that the grouting pressure p_c is 4 MPa, the depth of the pile shaft H is 40 m, the radius of the pile r_0 is 0.5 m, the thickness of the mud skin along the pile shaft b is 0.01 m, the volume of the grouting material q is 0.1 L/s, the consistency coefficient of the grouting material K is 0.5 kPa · s, and the yield stress of the grouting material τ_0 is 2 Pa. The relationships between the GMH and rheological indices are shown in Fig. 5. Ruan [48] studied the basic properties of the grouting material by experiments, whose results showed that the rheological index n corresponding to the water cement ratio of 0.5 to 0.7 was less than 0.1 in practical engineering. It shows that the GMH decreases with the rheological index gradually in Fig. 5. The category of the soil along the pile shaft has a great influence on the GMH. The GMH of the clay is the largest, the GMH of the silt is secondly, and the GMH of the gravel is the smallest, which is possible to show that the GMH has a great relationship with the seepage coefficient of the rock and soil.

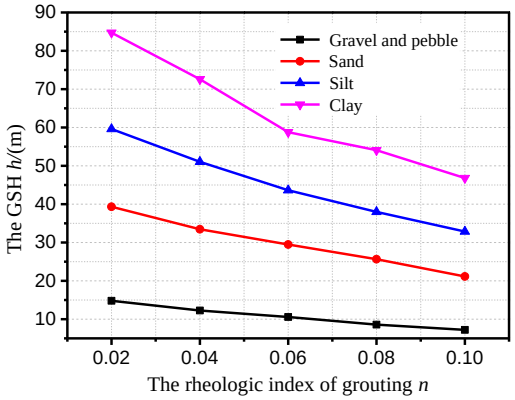

Fig. 5. The relationship curve between the GMH and the rheological index.

4.2. The relationship between the consistency coefficient and the GMH

The grouting parameters are assumed that the grouting pressure p_c is 4 MPa, the depth of the pile shaft H is 40 m, the radius of the pile r_0 is 0.5 m, the thickness of the mud skin along

Preprints (www.preprints.org) | NOT PEER-REVIEWED | Posted: 1 September 2021 doi:10.20944/preprints202109.0011.v1

the pile shaft b is 0.01 m, the volume of the grouting material q is 0.1 L/s, the rheological index n is 0.1, and the yield stress of the grouting material τ_0 is 2 Pa. The relationship curves between the GMH and the consistency coefficient K of the grouting material are shown in Fig. 6. The GMH decreases with the consistency coefficient gradually, which indicates that the GMH is closely related to the consistency coefficient of the grouting material. When the consistency coefficient K of the grouting material is less than 0.6 kPa · s, the GMH varies significantly. When the consistency coefficient K of the grouting material is greater than 0.6 kPa · s, the change of the GMH is small.

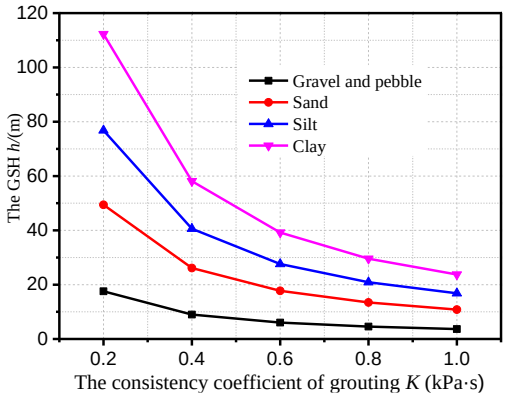

Fig. 6. The relationship curve between the GMH and the consistency coefficient K of the grouting material.

4.3. The relationship between the grouting pressure and the GMH

The grouting parameters are supposed that the depth of the pile shaft H is 40 m, the radius of the pile r_0 is 0.5 m, the thickness of the mud skin along the pile shaft is 0.01 m, the volume of the grouting material q is 0.1 L/s, the consistency coefficient of the grouting material K is 0.5 kPa · s, the rheological index n is 0.1, and the yield stress of the grouting material τ_0 is 2 Pa. The relationship between the grouting pressure p_c and the GMH is shown in Fig. 7. The GMH increases with the grouting pressure, which shows the positive linear relationship between them. Under certain conditions, the GMH is closely related to the permeability coefficient of the rock and soil.

Preprints (www.preprints.org) | NOT PEER-REVIEWED | Posted: 1 September 2021 doi:10.20944/preprints202109.0011.v1

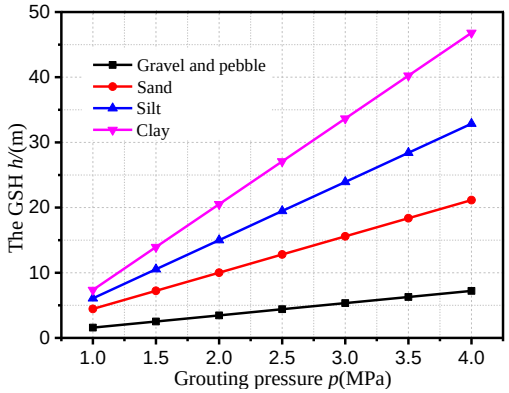

Fig. 7. The relationship curve between the GMH and the grouting pressure.

4.4. The relationship between the depth of the pile shaft and the GMH

The grouting parameters are supposed that the grouting pressure p_c is 4 MPa, the radius of the pile r_0 is 0.5 m, the thickness of the mud skin along the pile shaft is 0.01 m, the volume of the grouting material q is 0.1 L/s, the consistency coefficient of the grouting material K is 0.5 kPa · s, the rheological index n is 0.1, and the yield stress of the grouting material τ_0 is 2 Pa. The relationship between the GMH and the depth of the pile shaft H is shown in Fig. 8. The GMH decreases with the depth of the pile shaft H, which is the negative correlation between them. When the pile shaft is in the gravel layer, the influence of the depth of the pile shaft on the GMH is more obvious. When the pile body is in the clay, silt and sand layer, the depth of the pile shaft has little effect on the GMH.

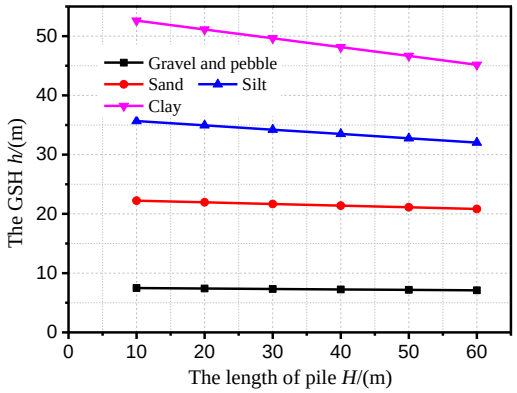

Fig. 8. The relationship curve between the GMH and the depth of the pile shaft.

4.5. The relationship between the pile diameter and the GMH

The grouting parameters are supposed that the grouting pressure p_c is 4 MPa, the depth of the pile shaft H is 40 m, the thickness of the mud skin along the pile shaft is 0.01 m, the volume of the grouting material q is 0.1 L/s, the consistency coefficient of the grouting material K is

Preprints (www.preprints.org) | NOT PEER-REVIEWED | Posted: 1 September 2021 doi:10.20944/preprints202109.0011.v1

0.5 kPa · s, the rheological index n is 0.1, and the yield stress of the grouting material τ_0 is 2 Pa. The relationship between the GMH and the diameter of the pile r_0 is shown in Fig. 9. The GMH decreases with the diameter of the pile, which indicates that the diameter of the pile has a greater influence on the GMH from Fig. 9.

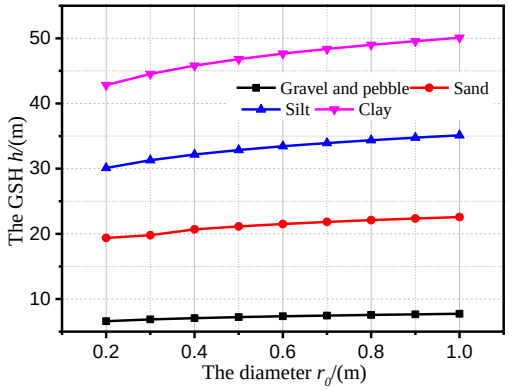

Fig. 9. The relationship curve between the GMH and the diameter of the pile.

4.6. The relationship between the thickness of the mud skin and the GMH

The grouting parameters are supposed that the grouting pressure p_c is 4 MPa, the depth of the pile shaft H is 40 m, the radius of the pile r_0 is 0.5 m, the volume of grouting material q is 0.1 L/s, the consistency coefficient of the grouting material K is 0.5 kPa · s, the rheological index n is 0.1, and the yield stress of the grouting material τ_0 is 2 Pa. The relationship between the GMH and the thickness of the mud skin b is shown in Fig. 10. The GMH increases with the thickness of the mud skin rapidly. For the bored cast-in-place concrete pile with the thick mud skin, the mud skin and soil can be strengthened by the post-grouted technology. The thicker the mud skin is, the better the grouting effect is.

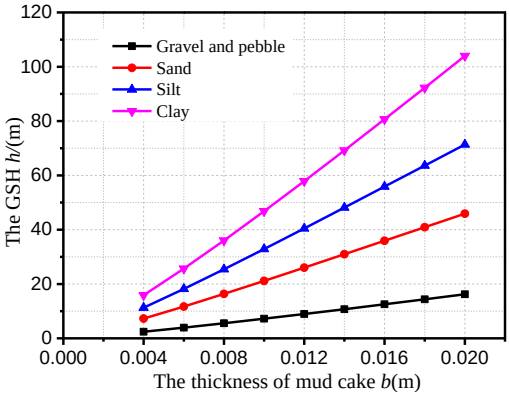

Fig. 10. The relationship curve between the GMH and the thickness of the mud skin.

It can be seen that the GMH of the gravel is always less than that of the sand, silt and clay

Preprints (www.preprints.org) | NOT PEER-REVIEWED | Posted: 1 September 2021 doi:10.20944/preprints202109.0011.v1

from Fig. 5 to Fig. 10. The reason may be that the permeability coefficient of the gravel is bigger, and the grouting pressure is easy to diffuse, which results in the smaller GMH. Nevertheless, the GMH of the clay is always higher than that of the sand, silt and clay. From this point of view, it shows that the clay is more conducive to the post-grouted technology.

5. The analysis of an engineering case

Referring to an engineering example in practical [49], the distribution of the soil layer along the pile shaft is shown in Table 3. The diameter and length of the test pile are 1.5 m and 41 m, respectively. The bearing stratum at the pile tip is the gravel, and the length of the pile is 8 m, which enters gravel stratum. The water-cement ratio of the grouting material is $W/C = 0.5 - 0.6$, and the average grouting pressure is about 4 MPa. When the foundation is excavated to 11m, the hardened cement ring with the thickness of 10-50 mm is found along the pile shaft, which indicates that the GMH along the pile shaft is about 30 m.

The calculation method deduced in this paper is used to calculate and analyze the GMH in this practical engineering. The grouting pressure p_c is 4 MPa, the volume of the grouting material q is 0.1 L/s, the thickness of the mud skin b is 0.01 m, the consistency coefficient K is 0.2 kPa · s and the rheological index n is 0.05. According to Equation (32), the GMH of the actual project is 27.6 m, which is close to the observative value of 30 m. The research results show that the conclusions derived in this paper are valid.

Table 3. The distribution table of layered soil along the pile shaft.

Classification of the soil layer	Buried depth of top surface (m)	Classification of the soil layer	Buried depth of top surface (m)
Miscellaneous fill	0	Silty clay	27.2
Plain Fill	0.2	Silty clay with sand	28.5
Sandy silt	1.2	Fine sand with gravel	35.8
Silt	7.8	Cobble and gravel	37.2
Sandy silt	10.2	Gravel	41.2
Silt	14.1	Cobble and gravel	44.5
Sandy silt	18.5	Gravel	50.2
Mucky silty clay	24.1	Cobble and gravel	58.5

6. Discussion

6.1. Hypothetical conditions

The Bingham model, the Carson model, the Power-law model and other two-parameter rheological models have better accuracy at high and medium shear rates. Nevertheless, the models

Preprints (www.preprints.org) | NOT PEER-REVIEWED | Posted: 1 September 2021 doi:10.20944/preprints202109.0011.v1

mentioned above are less effective at low shear rates. Most grouting material, especially polymer systems, have certain pseudo-plasticity. The actual rheological properties are quite different from the Carson model and Bingham model at lower shear rates, and is close to the Power-law model. Therefore, the Herschel-Bulkley model can better reflect the rheological characteristics of the actual grouting material. However, the Herschel-Bulkley model is more complex to use because it adds a parameter to traditional rheological models, such as the Carson model, the Bingham model and the Power-law model. The calculation of hydraulic parameters is complicated, which limits the application of the Herschel-Bulkley model in practical engineering.

It shows that there are usually three flow states when fluid flows in the pipeline, namely, the laminar flow, the transition flow and the turbulence flow. When other conditions are the same, the variation of the friction coefficient with the velocity is different. When calculating the pressure drop of the flowage frictional, the flow pattern of the fluid flow must be clearly defined so that the corresponding calculation method can be adopted. Because the flow pattern of the transition flow is very unstable, it is difficult to determine in the theoretical analysis and the experimental measurement. Therefore, the transition flow pattern is generally avoided and treated as the turbulent flow. Many dimensionless numbers are proposed to judge the end of the laminar flow in the theory, and the Reynolds number R_e is widely used in the engineering. When the Reynolds number R_e is larger than its critical value, the fluid is the turbulent flow, and otherwise, it is the laminar flow.

Because the mud skin layer is located between the pile and soil, its strength is lower than the rock and soil around the pile. Therefore, the grouting material squeezes the soil along the pile shaft under the action of the pressure and causes the interspace around the pile diameter. The grouting material will split and move upward along the weak surface, which will compact the mud skin and the soil around the pile shaft, or even destroy the mud structure. The grouting material fills voids after compaction and forms cement stones with the high strength after the consolidation, which enlarges the diameter of the pile. The movement of the grouting material in the weak layer can be summarized as follows: splitting the weak surface → the grouting material rising → compaction → re-splitting → re-rising → re-compaction. The above process is not categorized by the chronological order, and these processes may occur simultaneously in fact.

6.2. Further correction of the GMH

Preprints (www.preprints.org) | NOT PEER-REVIEWED | Posted: 1 September 2021 doi:10.20944/preprints202109.0011.v1

The GMH is related to the thickness and strength of the weak layer, the grouting ability, the grouting pressure and the volume of the grouting material. The grouting material is easy to diffuse in the soil layer with good grouting ability, and the grouting pressure is low, which causes the smaller GMH. The grouting is difficult to diffuse in the soil layer with poor grouting ability, and the grouting pressure is high, which causes the bigger GMH. The thicker the thickness of the weak layer is, the smaller the resistance force is, and the higher the GMH is. The pore water pressure increases when the soil is subjected to the grouting pressure. When the pore water pressure dissipates after grouting, the strength of the soil around the pile shaft increases due to compaction.

Considering the actual situation of the grouting pressure at the pile tip, the GMH should be revised to make the calculation more exact. The grouting pressure at the pile tip is generally less than that measured on the ground. Therefore, considering the loss of the grouting pressure during transportation, the grouting pressure measured on the ground should be re-estimated

$$P_e = k_1 P_m, \tag{33}$$

where P_e is the grouting pressure at the pile tip, P_m is grouting pressure measured on the ground, and k_1 is the correction coefficient of the grouting pressure considering the loss of the grouting pressure during transportation.

The parameter k_1 can be obtained by the ratio of the grouting pressure measured at the pile tip and the grouting pressure measured on the ground, whose value is in the range of 0.3-0.95.

As to the bored cast-in-place concrete pile in the practical engineering, the profile of the pile shaft is not regular cylindrical surfaces. The flow distance of the grouting material along the profile of the pile shaft will increase significantly, which will reduce the GMH. Therefore, the GMH calculated by Equations (30) and (32) should be reduced. The roughness coefficient of the pile shaft k_r is introduced, and the GMH is as follows

$$h' = k_r h, \tag{34}$$

and

$$k_r = L_{bp}/L_v, \tag{35}$$

where h' is the GMH considering the concave and convex of the pile shaft, k_r is the roughness coefficient of the pile shaft and it satisfies the condition $k_r \geq 1$, L_{bp} is the total length of the profile of the pile shaft, and L_v is the vertical height of the pile.

6.3. Suggestions for the further study

(1) Studying the mechanism of the grouting-soil interaction. The action mode of the

 doi:10.20944/preprints202109.0011.v1

grouting-soil is an important factor affecting the soil reinforcement and an important prerequisite for analyzing the reinforcement mechanism. Nonetheless, the distinction between the action modes of the grouting-soil interaction is vague or insufficient. The grouting method can be divided into the seepage grouting, the compaction grouting and the splitting grouting based on the mechanism of the grouting material diffusion. The above classification is based on the relationship between the grouting-soil interaction under ideal conditions. However, two or three grouting methods may exist simultaneously in the actual grouting engineering. Therefore, the conditions for the existence of the grouting-soil interaction and its transformation process should be understood and mastered in detail.

(2) Establishing a reasonable model to simulate the mechanism of the grouting material at the pile tip. The grouting process involves the interaction of the pile, the soil and the grouting material. The stress and deformation between the pile, the soil and the grouting material are non-linear. What's more, the heterogeneity of the material is very prominent and the boundary conditions are complex. The facts mentioned above make the traditional method to simulate the grouting at pile tip very different from the realities and lose the theoretical guiding significance. Therefore, it is necessary to find a new and reasonable mathematical model to simulate the grouting at the pile tip.

(3) Study on the bearing behavior of the PGDS. After grouting at the end of the pile, the resistance forces of the pile shaft and the pile tip have varying degrees of improvement. How to analyze and establish the bearing characteristics of the bored cast-in-place cement pile after grouting and the distribution law of the side friction and end resistance of the pile through the simple and reliable test and the relevant data of the grouting process. There are many methods to evaluate the grouting effect, and most of them are judged qualitatively, which are lack of the unified criteria for quantification. The quantitative evaluation criteria, which are reliable and identical, and meet different engineering requirements, should be further studied.

7. Conclusion

Based on the Herschel-Bulkley model and the basic equation of uniform flow, the analytical solutions of the grouting material diffusion along the aperture between the pile and soil are derived. Meanwhile, the parameters, such as the rheological index of the grouting material, the consistency coefficient of the grouting material, the length of the pile, the diameter of the pile, the thickness of the mud skin and the grouting pressure, are analyzed. The analyses shows that these

parameters have significant influences on the calculated result of the GMH. In practical engineering, therefore, these factors should be considered comprehensively for calculating the GMH to reduce the hidden risk of engineering. Besides, aiming at the GMH in layered soil, the iterative method for calculating the GMH is proposed through the study of the soil stratification around the pile shaft. An engineering example verifies the applicability of this method.

Author Contribution： In the process of this paper, each author is responsible for the following tasks. M.S. Gan Nan drafted the manuscript. Ph.D. Haiming Liu conceived and designed the research. Ph.D. Yanjie Zhang helped perform the analysis with constructive discussions. Wenyun Ding performed the data analyses. Ph.D. Jing Cao provided and analysed engineering background. Ph.D. Rongtao Yan collected important background information. All authors read and approved the final manuscript.

Funding： This paper is supported by the National Natural Science Foundation of China (Grant No. 51764020; 41967035), the Scientific Research Fund of Institute of Engineering Mechanics, China Earthquake Administration (Grant No. 2020EEEVL0204) and Yunnan Applied Basic Research Program (Grant No. 202001AT070083). The authors would like to thank them for providing financial support for conducting this research.

Institutional Review Board Statement: Not applicable.

Informed Consent Statement: Not applicable.

Data Availability Statement: Not applicable.

Acknowledgments: The authors sincerely thank the reviewers who contributed their expertise and time for reviewing this manuscript.

Declaration of Competing Interest

None.

References

1. Gao, G.Y.; Gao, M.; Chen, Q.S.; Dai, G.L. Field load testing study of vertical bearing behavior of a large diameter belled cast-in-place pile. *KSCE. J. Civ. Eng*. **2019**, 23, 2009-2016.。
2. Zhao, G.Q.; Yang, Y.Y.; Zhang, H.Q. A case study integrating field measurements and numerical analysis of high-fill slope stabilized with cast-in-place piles in Yunnan, China. *Eng. Geo.* **2019**, 253, 160-170.
3. Akguner, C.; Kirkit, M. Axial bearing capacity of socketed single cast-in-place piles. *Soils. Found*. **2012**, 52, 59-68.
4. Duan, X.S.; Kulhawy, F.H. Tip post-grouting of slurry-drilled shafts in soil: Chinese experiences. *Int. Found. Congr. & Equip. Expo*. **2009**, 47-54.
5. Mullins, G.; Winters, D.; Steven, D. Predicting end bearing capacity of post: Grouted drilled shaft in

cohesionless soils. *J. Geotech. Geoenvi. Eng*. **2006**, 132, 478-487.

6. Safaqah, O.; Bittner, R.; Zhang, X.G. Post-grouting of drilled shaft tips on the Sutong bridge: a case study. *Am. Soc. Civil. Eng. Geo-Denver. 2007 – Denver. Colorado. United. States.* **2007**, 1-10.
7. Fang, K.; Zhang, Z.; Zou, J.; Wang, Z. Laboratory studies on pressure filtration in post-grouting of drilled shaft tips in clay. *Geotech. Test. J*. **2012**, 32, 665-671.
8. Bolognesi, A.J.L.; Moretto, O. Stage grouting preloading of large piles on sand, Proc. 8th. *Int. J. Rock. Mech. Min. Sci. &. Geomech.* **1973**, 19-25.
9. Choi, Y.Y.; Lee, M.H.; Nam, M.S.; Kim, T.H. Development and implementation of a high-pressure, double-acting, bi-directional loading cell for drilled shafts. *Geotech. Test. J.* **2016**, 39, 196-205.
10. Littlejohn, G.S.; Ingle, J.L.K. Dadasbilge, Improvement in base resistance of large diameter piles founded in silty sand. *Proc. 8th. Eur. Conf. soil. mech. Found. Eng. Helsinki*. **1983**, 153-156.
11. Karimi, A.H.; Eslami, A. Physical modelling for pile performance combined with ground improvement using frustum confining vessel. *Int. J. Phys. Modell. Geotech*. **2018**, 18, 162-174.
12. Karimi, A.H.; Eslami, A.; Zarrabi, M. Study of pile behavior by improvement of confining soils using frustum confining vessel. *Sci. Iranica*, **2017**, 24, 1874-1882.
13. Fleming, W.G.K. The Improvement of pile performance by base grouting. *Proc. Inst. Civ. Eng. Civ. Eng.* **1993**, 97, 88-93.
14. Zhang, Z.M.S.; Wu, M.; Bao, F. Study of mechanism and application on bored pile tip grouting. *Chin. J. Geotech. Eng.* **1999**, 21, 681-686. (In Chinese)
15. Shen, B.H. Post grouting piles technique (2): Techinque of pressure grouting at base of slurry-drilled piles. *Ind. Constr*. **2001**, 31, 72-74. (In Chinese)
16. Tan, Y.Y.; Lan, H.L. Full-scale load testing of 75-90-m-long post-grouted drilled shafts in Suzhou stiff clay. *J. Test. Eval.* **2019**, 47, 284-309.
17. Zhou, J.L.; Zhang, J.W.; Wang, Y.Z.; Oh, E. Field static load tests of post-grouted piles under various failure conditions. *Adv. Civ. Eng.* **2020,** 1-18.
18. Kong, G.Q.; Wen, L.; Liu, H.L.; Zheng, J.J.; Yang, Q. Installation effects of the post-grouted micropile in marine soft clay. *Acta. Geotech*. **2020**, 15, 3559-3569.
19. Mullins, G.; Dapp, S.; Frederick, E.; Wagner, R. Post grouting drilled shaft tips: Phase I. *Confining. Pressure*. **2001**, 127-156.
20. Zhang, Z.T.; Gong, W.M.; Dai, G.L.; Xu, J. Enhancement of load bearing of post-grouted drilled shafts based on in situ tests. *Arabian J. Geosci.* **2021**, 14.
21. Wan, Z.H.; Dai, G.L.; Gong, W.M. Field and theoretical analysis of response of axially loaded grouted drilled shafts in extra-thick fine sand. *Can. Geotech. J.* **2020**, 57, 391-407.
22. Ng, C.W.W.; Li, J.H.M.; Yau, T.L.Y. Behavior of large diameter floating bored piles in saprolitic soils. *Soils. Found.* **2001**, 41, 37-52.
23. Khazaei, J.; Eslami, A. Postgrouted helical piles behavior through physical modeling by FCV. *Mar. Georesour. & Geotechnol.* **2017**, 35, 528-537.
24. Zhang, Q.Q.; Zhang, Z.M.; Li, S.C. Investigation into skin friction of bored pile including influence of soil strength at pile base. *Mar. Georesou. & Geotechnol.* **2013**, 31, 1-16.
25. Zhang, Z.M.; Yu, J.; Zhang, G.X.; Zhou, X.M. Test study on the characteristics of mudcakes and in situ soils around bored piles. *Can. Geotech. J.* **2009**, 46, 241-255.
26. Thiyyakkandi, S.; McVay, M.; Lai, P. Experimental group behavior of grouted deep foundations. *Geotech. Test. J.* **2014**, 37.
27. Youn, H.; Tonon, F. Numerical analysis on post-grouted drilled shaft: a case study at the Brazo River Bridge.

Comput. Geotech. **2010**, 37, 456-465.

28. Andersen, K.H.; Rawlings, C.G.; Lunne, T.A.; By, T.H. Estimation of hydraulic fracture pressure in clay. *Can. Geotech. J.* **1994**, 31, 817-828.
29. Panah, A.K.; Yanagisawa, E. Laboratory studies on hydraulic fracturing criteria in soil. *Soils. Found.* **1989**, 29, 14-22.
30. Alfaro, M.C.; Wong, R.C.K. Laboratory studies on fracturing of low-permeability soils. *Can. Geotech. J.* **2001**, 38, 303-315.
31. Li, P.; Zhang, Q.S.; Zhang, X.; Li, S.C.; Zuo, J.X. Grouting diffusion characteristics in faults considering the interaction of multi-sequence grouting. *Int. J. Geomech*. **2016**, 17, 1-10.
32. Cheng, W.C.; Ni, J.C.; Shen, J.S.; Wang, Z. Modeling of permeation and fracturing grouting in sand: laboratory investigations. *J. Test. Eval*. **2018**, 46, 2067-2082.
33. Marchi,M.; Gottardi, G.; Soga, K. Fracturing pressure in clay. *J. Geotech. Geoenv. Eng.* **2013**, 140.
34. Tani, M.E. Grouting rock fractures with cement grout. *Rock Mech. Rock. Eng.* **2012**, 45, 547-561.
35. Li, S.C.; Zhang, W.J. Zhang, Q.S.; Zhang, X.; Liu, R.T.; Pan, G.M.; Li, Z.P.; Che, Z.Y. Research on advantage-fracture grouting mechanism and controlled grouting method in water-rich fault zone. *Rock. Soil. Mech*. **2014**, 35, 744-752. (In Chinese)
36. Zou, J.F.; Li, L.; Yang, X.L. Penetration radius and pressure attenuation law in fracturing grouting *J. Hydraulic. Eng.* **2006**, 37, 314-319. (In Chinese)
37. Zhang, Z.M.; Zou, J. Penetration radius and grouting pressure in fracture grouting. *Chin. J. Geotech. Eng.* **2008**, 30, 181-184. (In Chinese)
38. Yang, J.Y.; Cheng, Y.H.; Chen, W.C. Experimental study on diffusion law of post-grouting slurry in sandy soil. *Adv. Civ. Eng*. **2019**.
39. Murdoch, L.C. Hydraulic fracturing of soil during laboratory experiments part I: Methods and observations. *Geotech.* **1992**, 43, 255-265.
40. Bezuijen, A.; Grotenhuis, R.T.; Tol, A.F.V.; Bosch, J.W.; Haasnoot, J.K. Analytical model for fracture grouting in sand. *J. Geotech. Geoenv. Eng.* **2011**, 137, 611-620.
41. Chen, T.; Zhang, L.; Zhang, D. An FEM/VOF hybrid formulation for fracture grouting modeling. *Comput. Geotech.* **2014**, 58, 14-27.
42. Zhou, L.; Su, K.; Wu, H.G.; Shi, C. Numerical investigation of grouting of rock mass with fracture propagation using cohesive finite elements. *Int. J. Geomech.* **2018**, 18.
43. Xiao, F.; Shang, J.L.; Zhao, Z.Y. DDA based grouting prediction and linkage between fracture aperture distribution and grouting characteristics. *Comput. Geotech.* **2019**, 112, 350-369.
44. Mohajerani, S.; Baghbanan, A.; Wang, G.; Forouhandeh, F. An efficient algorithm for simulating grout propagation in 2D discrete fracture networks. *Int. J. Rock Mech. Min. Sci.* **2017**, 98, 67-77.
45. Huilgol, R.R.; You, Z. Application of the augmented Lagrangian method to steady pipe flows of Bingham, Casson and Herschel–Bulkley fluids. *J. Non-Newtonian. Fluid. Mech.* **2005**, 128, 126-143.
46. Marchesini, F.H., Oliveira, R.M.; Althoff, H.; Mendes, P.R.D. Irreversible time-dependent rheological behavior of cement slurries: Constitutive model and experiments. *J. Rheol.* **2019**, 63, 247-262.
47. Huang, X. Marcelo, H.G. A Herschel-Bulkley model for mud-flow down a slope. *J Fluid Mech*. **1998**, 374, 305-333.
48. Ruan, W.J. Research on diffusion of grouting and basic properties of grouts. *Chin. J. Geotech. Eng*. **2005**, 27, 69-73. (In Chinese)
49. Zhang, Z.M.; Zou, J.; Liu, J.W.; He, J.Y. Theoretical study of climbing height of grout in pile-bottom base grouting. *Rock. Soil. Mech.* **2010**, 31, 2535-2540. (In Chinese)